

Graviton Phenomenology of Linear Dilaton Geometries

Masha Baryakhtar¹

*Stanford Institute for Theoretical Physics, Department of Physics,
Stanford University, Stanford, CA 94305*

Abstract

Five-dimensional geometries with a linearly varying dilaton background arise as gravity duals of TeV Little String Theories (LSTs) and provide a solution of the hierarchy problem through extra dimensions. The unique Kaluza-Klein graviton spectrum has a mass gap on the order of the dilaton slope followed by a closely spaced discretum of states. We study in detail the graviton phenomenology in this scenario, allowing the dilaton slope to vary from the MeV to the TeV scale. When the dilaton slope is large enough so that individual KK resonances can be resolved at the LHC, several of them can be discovered simultaneously and allow for the linear dilaton geometry to be uniquely identified. For much smaller values of the dilaton slope, the LHC signatures become similar to the 5-d ADD scenario while relaxing the astrophysical and experimental constraints. Due to the mass gap, the KK modes are produced on-shell and decay inside the LHC detector, modifying the diphoton and dilepton spectra at large invariant mass. Finally, we perform a similar analysis for the low curvature RS geometry. We present experimental limits and calculate the ultimate reach of a 14 TeV LHC for all the above scenarios.

arXiv:1202.6674v1 [hep-ph] 29 Feb 2012

¹email: mbaryakh@stanford.edu

Contents

1	Introduction	2
2	Hierarchy from Geometry	4
3	High Curvature ($\alpha \sim M_5$)	6
3.1	Phenomenology	6
3.2	Detection	7
4	Low Curvature ($\alpha \ll M_5$)	8
4.1	Physics of Low Curvature Linear Dilaton	8
4.2	Astrophysical Bounds	11
4.2.1	Supernovae	11
4.2.2	Big Bang Nucleosynthesis	14
4.3	Fixed Target Experiments	15
4.4	Large Hadron Collider	18
4.4.1	Low Curvature Searches	18
4.4.2	Future Reach	21
5	Low Curvature Randall-Sundrum	22
6	Discussion and Conclusions	23
7	Acknowledgements	24

1 Introduction

One of the most compelling connections between the weak scale and the Planck scale appears in the framework of extra dimensions, in which the fine-tuning problem becomes a question of dynamics and geometry [1,2]. In particular, in string theory the 4-dimensional Planck scale is not uniquely set by the string scale M_s , but also depends on the string coupling g_s and the internal volume of the six compactified dimensions V_6 ,

$$M_{Pl}^2 = \frac{1}{g_s^2} M_s^8 V_6. \tag{1}$$

Thus, there are two avenues to explain the weakness of gravity while keeping the string scale near a TeV: the large size of extra dimensions V_6 , which dilute the strength of gravity on the infrared brane [1], or the smallness of the string coupling constant g_s . The latter can be achieved in a controlled limit in the case of Little String Theories (LSTs) [3].

Little String Theories are 6-d strongly coupled non-Lagrangian theories generated by stacks of NS5 branes. The LSTs are dual to a local 7-d theory with a linearly varying dilaton background in the infinite 7th dimension. To obtain a finite 4-d Planck mass we use a 5-d compactification of

this geometry introduced in [4], in which the infinite linear dilaton extra dimension is terminated with two branes to a size r_c and two more extra dimensions are compactified on a smaller scale. Existing UV motivated extra-dimensional frameworks are the ADD flat compactification and the near-horizon limit of stacks of D3 branes which gives rise to Randall-Sundrum (RS) geometry [1,2]. The Linear Dilaton background, as the near horizon limit of stacks of NS5 branes, presents a third such possibility.

The dilaton gravity theory can be approximated by the bulk action

$$S = \int d^5x \sqrt{-g} e^{-\frac{\Phi}{M_5^{3/2}}} (M_5^3 R + (\nabla\Phi)^2 - \Lambda), \quad (2)$$

with the Standard Model on the $x_5 \equiv z = 0$ brane and the Planck brane at $z = r_c$. The linear dilaton solution is achieved by imposing the linearly varying background $\Phi/M_5^{3/2} = \alpha|z|$, with the bulk metric solution

$$ds^2 = e^{-\frac{2}{3}\alpha|z|} (\eta_{\mu\nu} dx^\mu dx^\nu + dz^2). \quad (3)$$

This geometry gives rise to a gapped Kaluza-Klein (KK) graviton spectrum with a massless graviton and the first mode of the KK tower appearing at $|\alpha|/2$:

$$m_n = \frac{|\alpha|}{2} \sqrt{1 + \frac{4n^2\pi^2}{(\alpha r_c)^2}}. \quad (4)$$

To further study the observable consequences of the gravitational sector we adopt the 5-d linear dilaton geometry without considering other states such as strongly coupled little string excitations that may be present in the LST.

In the Little String Theory context, the linear dilaton slope α is set by the number N of NS5 branes and for small N is naturally close to the 5-d Planck scale M_5 . In this study we consider the slope α as a free parameter which controls the mass scale of the KK modes. We compute the detailed experimental consequences at high curvature, $|\alpha| \sim M_5$; this scenario has the distinctive signature of many closely spaced resonances with decay modes to jets, leptons, and photons.

In addition, the limit of a low curvature 5th dimension reopens the exciting possibility of discovering one large ‘flat’ extra dimension at the Large Hadron Collider (LHC). High-energy collisions at the LHC are insensitive to the small curvature, so the phenomenology is very similar to that of ADD with one extra dimension. With zero curvature one extra dimension runs into severe astrophysical limits in addition to being ruled out by everyday observation: the size would need to be close to the Earth-Sun distance in size to result in a TeV-scale 5-d Planck mass [1]. A low curvature possibility was previously considered in [5]: an RS-type extra dimension with small 60 MeV curvature appears as flat at the LHC but reduces the physical size of the extra dimension needed to solve the hierarchy problem and avoids astrophysical bounds that rule out one large extra dimension. The linear dilaton geometry provides an alternative framework for this scenario.

This paper is organized as follows. In Section 2 we analyze the Kaluza-Klein mass spectra and the emergence of the hierarchy as a function of geometry in Randall-Sundrum and Linear Dilaton (LD) type backgrounds. Next, we examine the theory in several different regions of

parameter space. We discuss the case of high curvature and corresponding LHC bounds and reach in Section 3. In Section 4, we focus on the “large N ” limit, treating the curvature α as a free parameter. We present relevant astrophysical and laboratory constraints, deriving limits on α and the 5-dimensional Planck scale M_5 . In Section 4.4 we compute the LHC signals and study the current data for the low curvature $|\alpha| \ll M_5$ limit. We obtain experimental bounds and comment on optimal LHC searches and future reach of the collider. In Section 5 we discuss the low curvature RS geometry and apply experimental constraints to this spectrum. In Section 6 we summarize our findings and present searches to distinguish the Linear Dilaton geometry with experiment, as well as comment on its limitations in the context of Little String Theory at a TeV.

2 Hierarchy from Geometry

In both Randall-Sundrum and Linear Dilaton geometries, the curvature in the 5th dimension is crucial to both the low-energy phenomenology of the theory and to understanding the solution to the hierarchy problem. In this section we relate the relevant quantities in the two theories to develop intuition for curved geometries and their phenomenology.

The well-known RS metric is given by

$$ds_{RS}^2 = e^{-2k|y|} \eta_{\mu\nu} dx^\mu dx^\nu + dy^2, \quad (5)$$

where x^μ are the 4-dimensional coordinates and y is the physical distance along the extra dimension. The finite extra dimension is bounded by a UV brane at $y = 0$ and IR brane at $y = b$, and all scales are referenced to the UV brane.

The conformally flat form of (5) follows from the coordinate transformation $\frac{dz}{1+k|z|} = dy$,

$$ds_{RS}^2 = \frac{1}{(1+k|z|)^2} (\eta_{\mu\nu} dx^\mu dx^\nu + dz^2). \quad (6)$$

We can compare this conformally flat form directly to the linear dilaton metric [4],

$$ds_{LD}^2 = e^{-\frac{2}{3}\alpha|z|} (\eta_{\mu\nu} dx^\mu dx^\nu + dz^2), \quad (7)$$

where as in RS the extra dimension z is finite and compactified on an orbifold with Z_2 symmetry. In this case all parameters are defined with respect to the IR brane at $z = 0$ which contains the Standard Model fields; the UV brane is at $z = r_c$. For a given 5-d Planck mass M_5 and slope α of the dilaton field the size of the extra dimension r_c is fixed by the hierarchy between the 4-d M_{Pl} and 5-d Planck mass scales:

$$M_{Pl}^2 = 2 \int_0^{r_c} dz e^{-\alpha|z|} M_5^3 = -2 \frac{M_5^3}{\alpha} (e^{-\alpha r_c} - 1). \quad (8)$$

This relation also fixes $\alpha < 0$. For typical values $M_5 = 1 \text{ TeV}$ and $|\alpha| = 1 \text{ GeV}$, we see that $|\alpha r_c| = 60$ and the quantity $|\alpha r_c|$ depends only logarithmically on α and M_5 for a fixed value of the hierarchy between M_{Pl} and M_5 .

In the RS geometry (6), the change of mass scales along the bulk can be understood as the running of the cutoff in the dual CFT theory [6]. The model with a linearly varying dilaton background is not scale invariant and the dual theory is strongly coupled, so a similar analysis is not possible here. Nevertheless, important analogies to RS phenomenology remain.

The warped geometry provides an explanation for the hierarchy between the weak scale and the Planck mass. We can see that mass scales are warped down on the IR brane relative to the UV brane in both RS and LD by considering the behavior of the Higgs vacuum expectation value (VEV). In RS, the induced 4-d metrics at the IR and UV branes are

$$\text{IR} : g_{\mu\nu}|_{y=b}^{RS} = e^{-2kb} \eta_{\mu\nu} \quad \text{UV} : g_{\mu\nu}|_{y=0}^{RS} = \eta_{\mu\nu}. \quad (9)$$

For a comparison to the LD geometry we rewrite the metric (7) in physical coordinates, $dy = e^{-\frac{1}{3}\alpha z} dz$,

$$ds_{LD}^2 = \left(1 + \frac{|\alpha y|}{3}\right)^2 \eta_{\mu\nu} dx^\mu dx^\nu + dy^2. \quad (10)$$

We see that the induced metrics on the two branes in LD are

$$\text{IR} : g_{\mu\nu}|_{y=0}^{LD} = \eta_{\mu\nu} \quad \text{UV} : g_{\mu\nu}|_{y=y_0}^{LD} = \left(1 + \frac{|\alpha y_0|}{3}\right)^2 \eta_{\mu\nu}. \quad (11)$$

Since the induced metric differs between branes in both cases, to compare the behavior of the mass scales we redefine the Higgs field to be canonically normalized, leading to a warped value of the VEV [2]. In RS the warping is exponential, $v_{IR} = e^{-kb} v_{UV}$, and in linear dilaton it is a power law, $v_{IR} = (1 + |\alpha y_0|/3)^{-1} v_{UV}$. In general, the Higgs VEV is warped down on the IR brane relative to the UV so the weak mass scale is suppressed compared to M_{Pl} .

Along with the hierarchy, geometry also determines the 4-d KK graviton mass spectra. This is clear if we rescale the metric perturbation $h_{\mu\nu}$ to write the graviton equation of motion in the form of a Schrodinger equation. In the LD model, the curvature acts as a mass term: the spectrum corresponds to that of a particle with mass $|\alpha|/2$ in a box of size r_c [4],

$$\eta^{MN} \partial_M \partial_N \tilde{h}_{\mu\nu}^{(n)} - \frac{\alpha^2}{4} \tilde{h}_{\mu\nu}^{(n)} = 0. \quad (12)$$

In RS on the other hand, the masses of the KK modes correspond to a massless particle in a potential: they are determined by Bessel function zeros corresponding to solutions of the potential $V(y)$ [2],

$$\eta^{MN} \partial_M \partial_N \tilde{h}_{\mu\nu}^{(n)} - V(y) \tilde{h}_{\mu\nu}^{(n)} = 0. \quad (13)$$

The physical quantity that determines the graviton spectrum is the time it takes for light to travel from the UV to the IR brane. In the case of RS the time is at the TeV scale,

$$\Delta t_{RS}^{null} = \frac{e^{kb}}{k} \quad (14)$$

For LD, the time it takes for light to travel from UV to IR brane is just

$$\Delta t_{LD}^{null} = r_c \quad (15)$$

For $|\alpha| = 1 \text{ TeV}$, $r_c = 10^{-17} \text{ m}$, and even for a very low curvature $|\alpha| = 20 \text{ MeV}$, the proper size is small, $r_c = 10^{-12} \text{ m}$. Compare this to the physical size of the 5th dimension: in physical coordinates (10) the proper distance y_0 between the branes is of order $3|\alpha|^{-1}e^{\frac{|\alpha r_c|}{3}}$, which can be as large as $10 \mu\text{m}$ for $|\alpha| = 20 \text{ MeV}$. However, the mass spectrum (4) is determined by the inverse time it takes light to travel between the branes—in this case r_c^{-1} —as well as the curvature α , and not the proper length of the extra dimension y_0 . Since the graviton KK mass sets the scale of modification of the gravitational $1/r^2$ law, laboratory and astrophysical bounds that rule out a flat fifth dimension [7–11] have limited application to this scenario.

3 High Curvature ($|\alpha| \sim M_5$)

3.1 Phenomenology

In the 5-d linear dilaton compactified geometry, Standard Model fields are localized on the IR brane and the graviton propagates in the bulk. The equation of motion in the bulk corresponds to that of a free massive particle, which when compactified gives rise to a gapped mass spectrum in 4-d. The details of the compactification can be found in [4]. The mass spectrum is unique: the mass gap is set by the curvature α , with the first massive state at $m_1 = |\alpha|/2$, followed by a discretum of states spaced by r_c^{-1} with masses proportional to the curvature α ,

$$m_n = \frac{|\alpha|}{2} \sqrt{1 + \frac{4n^2\pi^2}{(\alpha r_c)^2}}. \quad (16)$$

Unlike condensed matter systems with ubiquitous mass gaps, the spectrum is very rare in gravity since gravitational interactions cannot be screened in positive-energy systems. In this case, a linearly varying dilaton provides a quadratic potential term for the modes in the extra dimension, resulting in a KK masses resembling the energy spectrum of a ‘massive particle in a box’ in 4-d.

Each KK mode couples to all Standard Model fields equally through the stress-energy tensor,

$$\mathcal{L} = -\frac{1}{M_{Pl}} h_{\mu\nu}^{(0)} T_{\mu\nu} - \frac{1}{\Lambda_n} h_{\mu\nu}^{(n)} T_{\mu\nu}. \quad (17)$$

The coupling of each mode n is given by the value of the graviton wavefunction at the TeV brane; the wave functions are localized close to the TeV brane so the couplings are much stronger than M_{Pl}^{-1} ,

$$\frac{1}{\Lambda_n} = \frac{|\alpha|^{1/2}}{M_5^{3/2}} \frac{1}{|\alpha r_c|^{1/2}} \left(\frac{4n^2\pi^2}{4n^2\pi^2 + (\alpha r_c)^2} \right)^{1/2}. \quad (18)$$

For large mode number n , the spacing of the modes is $\delta m = |\alpha|\pi/|\alpha r_c| \sim |\alpha|/20$. The coupling is mode-dependent and is additionally suppressed from $(\text{TeV})^{-1}$ by $(|\alpha|/M_5)^{1/2}$:

$$\Lambda_1 = (80 \text{ TeV}) \left(\frac{|\alpha|}{M_5} \right)^{1/2} \left(\frac{M_5}{\text{TeV}} \right)^{-1} \quad (19)$$

$$\Lambda_{n>100} = (8 \text{ TeV}) \left(\frac{|\alpha|}{M_5} \right)^{1/2} \left(\frac{M_5}{\text{TeV}} \right)^{-1}. \quad (20)$$

3.2 Detection

For large enough values of α , the spacing between modes ($\delta m \sim |\alpha|/20$) becomes larger than the invariant mass resolution of the LHC detectors. In this region of parameter space, experimental searches for KK resonances have potential reach. This is a true jackpot scenario — the modes are closely spaced, so upon seeing one resonance, the LHC would be able to detect a multitude of modes. The first hundred have a varying coupling strength and mass spacing, and once distinct resonances become visible, all the kinematically accessible modes will be seen above background after a factor of 3-5 increase in luminosity. This information, combined with a measurement of the unique mass gap, can help pinpoint the extra dimension as resulting from a Linear Dilaton background.

In particular, for $|\alpha| \sim 1 \text{ TeV}$, KK modes will have spacing above the muon resolution of the ATLAS and CMS detectors and can be seen as resonant peaks. At both detectors, muon tracks are reconstructed with 97% efficiency and an invariant mass resolution of 3-5% between 400 GeV and 2 TeV, with 4% at 1 TeV [12, 13]. An example invariant mass spectrum at the LHC in the dimuon channel is shown in Figure 1(a) for $|\alpha| = 1 \text{ TeV}$, $M_5 = 3 \text{ TeV}$: already at a 7 TeV LHC energy and 30 fb^{-1} of data, individual resonances begin to become visible above the background and detector resolution. For comparison, the low α spectrum in Figure 1(b) would appear as a continuous excess at the LHC detectors; it has the same energy dependence for any small value of the curvature (including zero curvature).

We can set bounds on this scenario from current LHC Randall-Sundrum resonance searches, which depend on the coupling strength and mass of each KK mode, as shown in Figure 2 [14–16]. These searches are sensitive to KK gravitons decaying to pairs of photons or leptons that can be seen as invariant mass peaks above the background. Similarly, extrapolating from RS reaches gives the reach regions for high α a center of energy 14 TeV and integrated luminosity of 100 fb^{-1} shown in Figure 2.

In addition to resonance searches, we consider bounds from the total cross-section increase due to the extra modes. The dominant contribution is from on-shell s -channel KK gravitons; the width of each resonance is much smaller than the mass difference between consecutive modes, and there is minimal interference with Standard Model particles. We model the production and decay of KK modes up to the cutoff M_5 for a range of $|\alpha|$ and M_5 in Madgraph 5.0 [17] and compare the signal cross-section as a function of center of mass energy with published limits [14–16, 18]. The dependence on the cutoff is insignificant due to the extremely low production rates at multi-TeV energies.

We find that we obtain more stringent bounds by including the highest mass ‘control’ region in

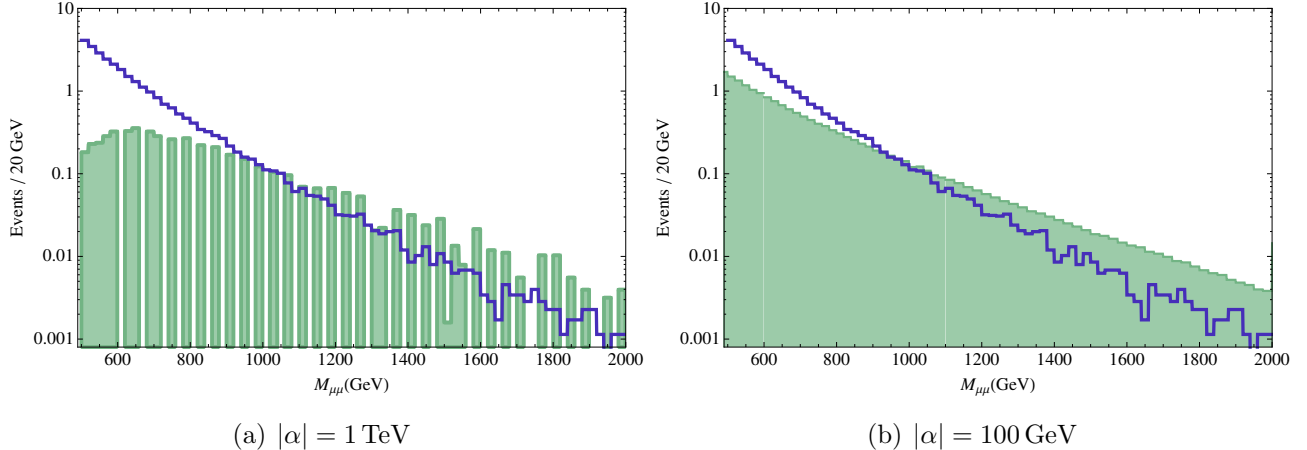


Figure 1: The invariant mass spectrum at the LHC in the dimuon channel after 30 fb^{-1} integrated luminosity at $\sqrt{s} = 7 \text{ TeV}$ for example spectra with (a) $M_5 = 3 \text{ TeV}$, $|\alpha| = 1 \text{ TeV}$, and (b) $M_5 = 3 \text{ TeV}$, $|\alpha| = 100 \text{ GeV}$. Green (gray): signal, blue (black): background. The data is grouped in 20 GeV bins; detector resolution ranges from 12 GeV at 400 GeV to 40 GeV at 1 TeV and 100 GeV at 2 TeV.

addition to the signal region. We obtain a limit $M_5 \gtrsim 3 \text{ TeV}$ for varying values of high curvature and no limit for $|\alpha| > 4 \text{ TeV}$; the leading order 95% CL limit is shown in Figure 2. The published information about systematic uncertainties is only available for the highest mass signal region so in calculating limits we have taken into account statistical uncertainty only; thus our limit is an overestimate. A full experimental analysis is required to obtain precise bounds.

4 Low Curvature ($|\alpha| \ll M_5$)

4.1 Physics of Low Curvature Linear Dilaton

An interesting aspect of the linear dilaton geometry is that it provides a natural framework for one large extra dimension with a small curvature. In the limit where the linear dilaton slope goes to zero, $\alpha \rightarrow 0$, the model reproduces ADD with one extra dimension. From the 4-d point of view, a small curvature α in the extra dimension lifts the spectrum of Kaluza-Klein (KK) gravitons and avoids standard laboratory and astrophysical constraints on large extra dimensions. In this section we show that there are no bounds on a TeV Planck scale from low energy tests for $|\alpha|$ as low as tens of MeV.

On the other hand, the high energy LHC is sensitive not to low energy details of the spectrum but to the entire discretum, so even with the mass gap the low α spectrum will be resolved as one extra dimension. Thus, there is potential to discover one large extra dimension at the LHC, a possibility so neglected that it does not appear in any experimental analyses. A similar phenomenological scenario has been pointed out and analyzed previously for a low curvature limit of RS in [5,19]. Still, the phenomenology is distinct: there is a lower density of modes than in ADD and each mode is more strongly coupled. For instance, there are no missing energy signatures

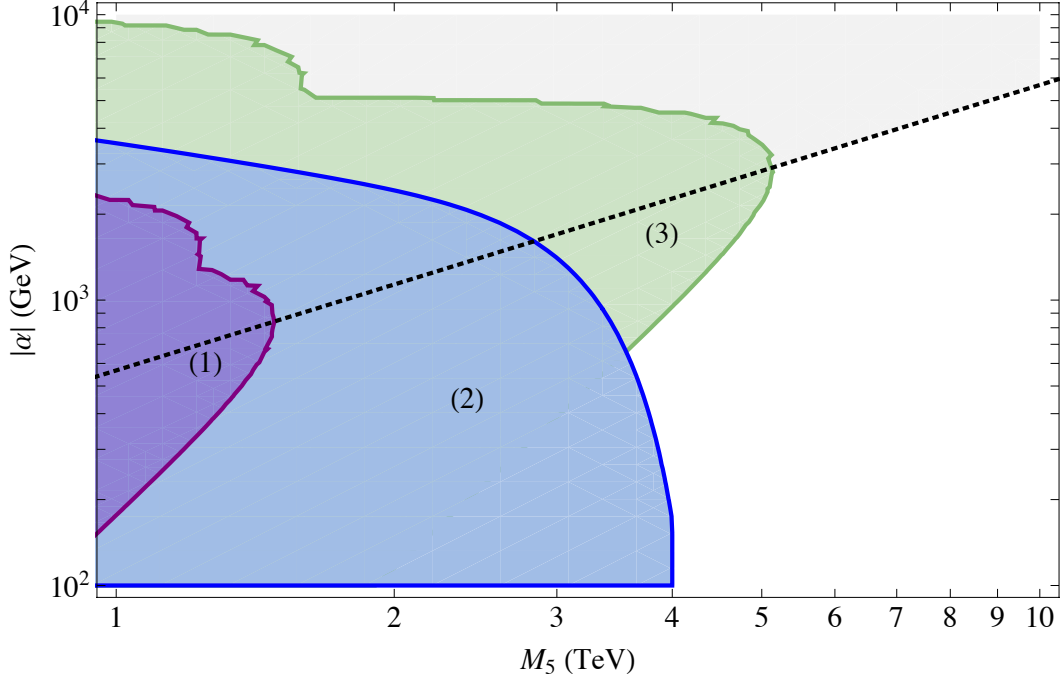


Figure 2: LHC limits on high curvature Linear Dilaton geometry. (1) Purple: current exclusion from RS resonance searches; (2) blue: current exclusion from ADD total cross-section searches; (3) green: LHC reach in resonance searches with $\sqrt{s} = 14$ TeV and 100 fb^{-1} integrated luminosity; gray (above dotted line): non-perturbative region where the curvature $|\alpha|$ becomes comparable to the 5-d Planck scale M_5 . Reach in M_5 is limited by weak coupling, while reach in $|\alpha|$ is limited by production of the first mode of mass $|\alpha|/2$.

because most KK modes have short lifetimes and decay inside the detector.

In the following sections we present the leading bounds on low α geometries, including emission in supernovae and BBN, fixed target experiments, and the latest experimental bounds from the LHC. The limits are shown in Figure 3.

In the $|\alpha| \ll M_5$ limit we consider in this section, the coupling Λ_n^{-1} of each individual mode is extremely weak:

$$\Lambda_1 = (8 \times 10^6 \text{ GeV}) \left(\frac{|\alpha|}{100 \text{ MeV}} \right)^{1/2} \left(\frac{M_5}{\text{TeV}} \right)^{-3/2} \quad (21)$$

$$\Lambda_{n>100} = (8 \times 10^5 \text{ GeV}) \left(\frac{|\alpha|}{100 \text{ MeV}} \right)^{1/2} \left(\frac{M_5}{\text{TeV}} \right)^{-3/2} \quad (22)$$

while the spacing of the modes is very small,

$$\delta m_n = 5 \text{ MeV} \left(\frac{|\alpha|}{100 \text{ MeV}} \right) \quad \text{for } n \gg 1. \quad (23)$$

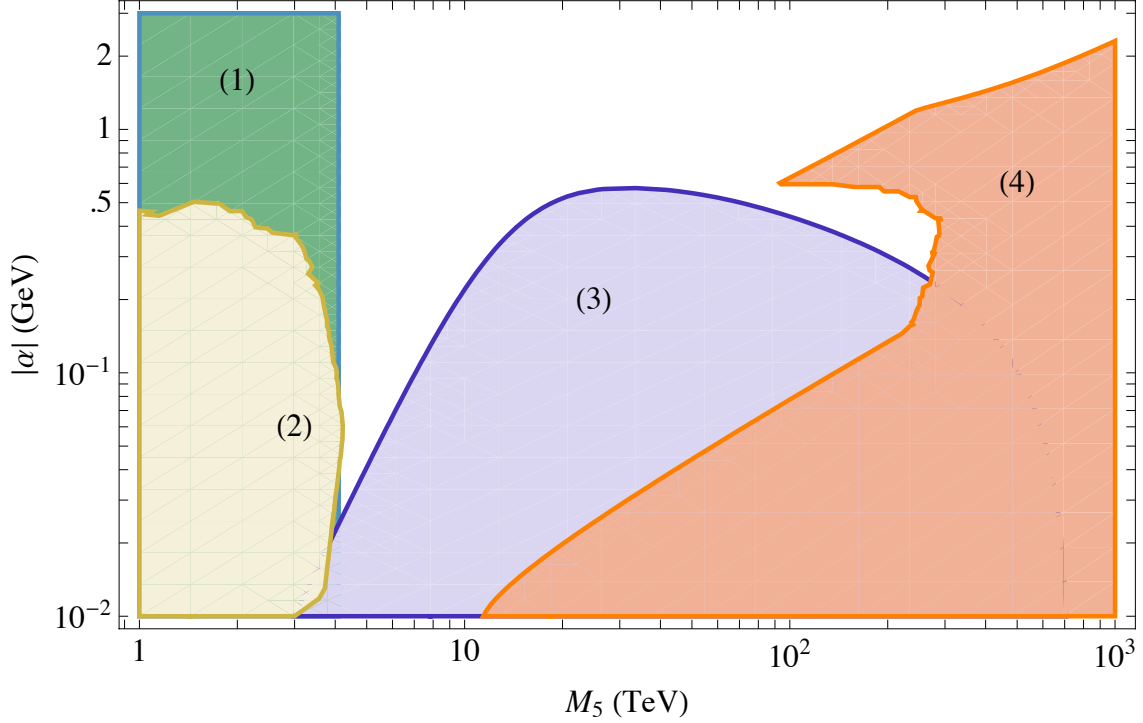


Figure 3: Current Bounds on Low Curvature Linear Dilaton. (1) Green: LHC limits at $\sqrt{s} = 7$ TeV after 2.2 fb^{-1} integrated luminosity, (2) yellow: 10 events in the E137 electron beam dump experiment (zero events were observed over the course of the experiment), (3) purple: energy flux from Supernova 1987A, (4) orange: BBN electromagnetic and hadronic bounds. The upper lobe in BBN exclusion results from hadronic limits, with a lower threshold at $|\alpha| \sim 600$ MeV when hadronic decay channels become available to the lightest KK mode.

Thus for many processes considered here, the contribution of a single mode is undetectable and we will be interested in the total cross-section where the entire discretum of modes participates in the process. To do so we can approximate the sum over modes as an integral,

$$\sum_n = \int dm \frac{r_c}{\pi} \frac{m}{(m^2 - \alpha^2/4)^{1/2}}. \quad (24)$$

Unlike the ADD and RS theories, in the linear dilaton geometry the coupling of each mode is a function of mode number (18). To compute total cross-sections we calculate the continuum integral of the sum $\sum_n \sigma_n$. Since the coupling is very weak, the leading production matrix elements contain single graviton couplings and are proportional to Λ_n^{-2} , which gives

$$\sum_n \Lambda_n^{-2} = \int dm \frac{1}{\Lambda(m)^2} = \frac{1}{\pi M_5^3} \int \frac{dm}{m} \left(m^2 - \frac{\alpha^2}{4} \right)^{\frac{1}{2}}. \quad (25)$$

In the $\alpha \rightarrow 0$ limit, the expression (25) reduces to the sum over modes in one flat extra dimension, up to a factor of 2π due to a difference in the definition of M_5 .^a While the cross-section of a single mode is proportional to $|\alpha|/M_5^{-3}$, the production cross-section for any mode is proportional to M_5^{-3} and independent of α given that all modes are accessible.

Another important quantity for understanding experimental signatures is the lifetime of the modes. The decay rate is

$$\Gamma_n = \frac{m_n^3}{320\pi\Lambda_n^2}k(m), \quad (26)$$

where $k(m)$ is a function of the spin and number of open decay channels (1 for fermions, 2 for bosons, etc.) [20]. Even for a fixed number of decay channels, the lifetime varies sharply with α and M_5 , as well as mode number:

$$\tau_1 = (3 \times 10^{-5} \text{ s}) \left(\frac{M_5}{\text{TeV}} \right)^3 \left(\frac{|\alpha|}{100 \text{ MeV}} \right)^{-4} \quad (27)$$

$$\tau_{100} = (4 \times 10^{-13} \text{ s}) \left(\frac{M_5}{\text{TeV}} \right)^3 \left(\frac{|\alpha|}{100 \text{ MeV}} \right)^{-4}. \quad (28)$$

Lifetimes shorter than 10^{-4} s may be possible to measure in laboratory experiments, while lifetimes longer than 1 s can have an impact on cosmology.

We consider the parameter space of the theory in the (α, M_5) plane (Figure 3). The 5-d Planck scale M_5 determines the strength of the coupling of the modes, while the curvature α sets both the mass spectrum and the coupling.

In sections 4.2 and 4.3, we present relevant astrophysical and laboratory constraints; we find the first KK mode can be as light as 10 MeV in LD and 1 MeV in low curvature RS and avoid all existing bounds for TeV-scale M_5 . Rare meson decays, such as $K^+ \rightarrow \pi^+ G$, could also potentially set limits on M_5 ; however, as these processes are loop suppressed, the resulting limits from meson experiments are much weaker than those due to fixed target experiments [21]. In Section 4.4 we compute the LHC phenomenology and obtain a leading order limit of $M_5 \gtrsim 4.1$ TeV and comment on optimal LHC searches and future reach of the collider.

4.2 Astrophysical Bounds

4.2.1 Supernovae

One of the strongest bounds on the Planck scale in ADD comes from overproduction of KK modes in Supernova 1987A [8–10]. The luminosity and duration of the SN1987A burst as measured by the observed neutrino flux limits the energy loss due to other weakly interacting light states to be less than $\dot{\epsilon} = 10^{19} \text{ erg g}^{-1} \text{ s}^{-1}$ at a typical supernova temperature of $T = 30 \text{ MeV}$ [22]. In the case of one flat extra dimension, the density of light KK states is very high and results in a strong limit: $M_5 > 7.4 \times 10^5 \text{ GeV}$ [10]. In the linear dilaton geometry, a quick estimate gives the

^aThe difference in conventions compared to flat extra dimensions appears in Eqn. (8), where the length of the extra dimension is defined to be r_c whereas it is often written as $2\pi R$.

same limit for $|\alpha| \ll T$ where the curvature is irrelevant, and no limit for $|\alpha|/2 > 30$ MeV, where the mass of first mode is above the SN temperature. However, we find the thermally suppressed emission of heavier gravitons as well as reabsorption in the SN core lead to a more interesting constraint, as we discuss below.

Graviton Emission The leading process for KK production is nuclear gravistrahlung – the radiation of a graviton G in the process of collision of two nucleons N ,

$$N + N \rightarrow N + N + G \quad (29)$$

Other processes such as $N + \gamma \rightarrow N + G$ and $e + \gamma \rightarrow e + G$ are suppressed by α_{EM} and give sub-leading contributions. For soft graviton emission, the process factorizes into the cross-section for nuclear scattering σ_N and the probability for graviton emission $T^2 \Lambda_n^{-2}$ where Λ_n^{-1} is coupling of the n^{th} mode. For a non-degenerate, non-relativistic nuclear medium of the neutron star, the energy loss rate for a single graviton is given by [10]

$$Q_m \propto \frac{1}{\Lambda(m)^2} \sigma_N n_B^2 T^{7/2} m_N^{-1/2} \quad (30)$$

where $\Lambda(m)$ is the graviton coupling, T is the neutron star core temperature, n_B is the baryon density in the star, and m_N is the nucleon mass. For typical neutron star conditions of $T = 30$ MeV and $\rho = 3 \times 10^{14}$ g cm $^{-3}$, $\sigma_N = 25$ mb is a good approximation for the nuclear cross-section.

We compute the total energy loss from a supernova through graviton emission in the soft graviton approximation. For one large extra dimension with radius R , the sum of the loss rates (30) over all modes approximated as an integral gives the energy loss rate Q [10]:

$$Q = \frac{2R}{(2\pi)^2} \int_0^\infty d\omega \omega S(-\omega) \int_0^\omega dm (\omega^2 - m^2)^{1/2} \left(\frac{19}{18} + \frac{11}{9} \frac{m^2}{\omega^2} + \frac{2}{9} \frac{m^4}{\omega^4} \right) \quad (31)$$

where the integrals over mass of the mode m and energy ω include the sum over graviton polarizations as well as integrals over momentum and energy with dispersion relation $k = (\omega^2 - m^2)^{1/2}$. $S(\omega)$ is a structure function up to first order in ω/T which is derived using the single graviton energy loss rate and the principle of detailed balance:

$$S(-\omega) = \frac{1}{\omega^2} \frac{2}{1 + e^{\omega/T}} \frac{1024\sqrt{\pi}}{5} \frac{\sigma_N n_B^2 T^{5/2}}{m_N^{1/2}} \frac{1}{\Lambda_n^2} \quad (32)$$

Applying this analysis to the linear dilaton geometry, the larger mass dependent coupling $\Lambda(m)^{-1}$ should be included in the integral over modes. The mode spacing is also larger at $\pi/r_c \sim \alpha/20$, but the spectrum can be still approximated as a continuum starting at the lightest mode of $\alpha/2$ for α up to 1 GeV. Then the expression for linear dilaton geometry is

$$Q = \frac{S_0}{(2\pi)^2 \pi M_5^3} \int_{\alpha/2}^\infty d\omega \frac{2}{1 + e^{\omega/T}} \int_{\alpha/2}^\omega dm G(m/\omega, \alpha/2m) \quad (33)$$

where

$$S_0 = \frac{1024\sqrt{\pi} \sigma_N n_B^2 T^{5/2}}{5 m_N^{1/2}} \quad (34)$$

and the integrand

$$G(m/\omega, \alpha/2m) = \left(1 - \frac{m^2}{\omega^2}\right)^{1/2} \left(1 - \frac{\alpha^2}{4m^2}\right)^{1/2} \left(\frac{19}{18} + \frac{11}{9} \frac{m^2}{\omega^2} + \frac{2}{9} \frac{m^4}{\omega^4}\right) \quad (35)$$

includes the mass-dependent coupling and reduces to the flat geometry (31) for $\alpha \rightarrow 0$. Evaluating the integral over m (33) with typical SN conditions, $T = 30$ MeV and $\rho = 3 \times 10^{14}$ g cm $^{-3}$, $\sigma_N = 25$ mb, and $n_B = 10^{-3}$ GeV 3 gives

$$Q = 3.78 \times 10^{41} \text{ erg cm}^{-3} \text{ s}^{-1} \left(\frac{T}{30 \text{ MeV}}\right) \left(\frac{M_5}{\text{TeV}}\right)^{-3} \mathcal{I}(\alpha/2T) \quad (36)$$

where the integral $\mathcal{I}(\alpha/2T)$ (with $x = \omega/T$),

$$\mathcal{I}(\alpha/2T) = \int_{\alpha/2T}^{\infty} dx \frac{x}{1+e^x} \frac{12}{\pi^2} \left(\frac{(\alpha/2T)^6}{50x^6} + \frac{(\alpha/2T)^4}{5x^4} + \frac{3(\alpha/2T)^2}{10x^2} - \frac{38(\alpha/2T)}{25x} + 1 \right) \quad (37)$$

is equal to 1 for zero curvature and accounts for thermal suppression of production for $\alpha > 0$. For $\alpha < 2T$, all modes are produced in nearly equal number below the temperature of the supernova so production is suppressed proportionally: $\mathcal{I}(0.1) = 0.9$ and $\mathcal{I}(0.5) = 0.5$ for example. If the lightest mode is heavier than the temperature, then production is suppressed exponentially.

To derive a bound on the geometry in terms of the $\alpha - M_5$ parameter space, we impose the condition that the energy carried away by gravitons is less than the total loss rate [22],

$$Q(\alpha/2T, M_5) < \dot{\epsilon}\rho = 3 \times 10^{33} \text{ erg cm}^{-3} \text{ s}^{-1}. \quad (38)$$

For $\alpha/2 \ll T$, the curvature is irrelevant and the bound on M_5 is the same as for 1 flat extra dimension, $M_5 \gtrsim 7.4 \times 10^5$ GeV. For $\alpha/2 \lesssim T$, the production is suppressed by the fraction of modes accessible below T . If the first mode is heavier than the supernova temperature, production is thermally suppressed and the limit on M_5 becomes much weaker; for $\alpha = 10T$, the suppression is 1/300. Still, at M_5 of a few TeV, the interaction cross-section is so large that even very thermally suppressed KK towers with $m_n \gtrsim 0.5$ GeV are experimentally excluded.

Graviton Absorption When a KK graviton is produced and then scatters in the NS core, it thermalizes and does not carry away energy. This process opens a window in parameter space at low M_5 where the KK interaction cross-section is highest. At the same time, at low M_5 , the coupling is large and KK modes are overproduced by a factor of $(7.4 \times 10^5 \text{ GeV}/M_5)^3$ at low α , so all but a small fraction of KK gravitons have to scatter before leaving the neutron star to satisfy the energy loss bounds.

The mean free path of the n^{th} mode is $L_n = (\sigma n_B)^{-1}$ where σ is the interaction cross-section and n_B is the baryon number density, $n_B = 10^{-3} \text{ GeV}^3$. The inverse gravistrahlung process, $N + N + G \rightarrow N + N$, gives

$$L_n = (\sigma n_B)^{-1} = (\Lambda_n/T)^2 (25 \text{ mb})^{-1} 10^3 \text{ GeV}^{-3} = 200 \text{ m} \left(\frac{M_5}{\text{TeV}} \right)^3 \left(\frac{\alpha}{100 \text{ MeV}} \right)^{-1} \quad (39)$$

The density of the neutron star is very high so there is negligible phase space suppression for the $3 \rightarrow 2$ process.

The cross-section for absorption is proportional to n^2 for the early modes so the first mode has the longest interaction length. Then a conservative bound on the fraction of modes that escape the supernova is $e^{-L_1/R_{SN}}$ where $R_{SN} \sim 10 \text{ km}$ is the radius of the star. In the excluded region in Figure 3, we take into account the varying interaction lengths weighted by the thermal distributions of modes. For the region in parameter space relevant to reabsorption, KK decay length is longer than interaction length and is not relevant. The absorption rate is within a factor of a few of more detailed estimates [10], which is the expected accuracy of both calculations.

Another bound on KK gravitons from supernovae arises when gravitons produced in a supernova are trapped in gravitational orbit around the neutron star. As the gravitons gradually decay, the decay products can hit the surface of the neutron star and reheat it, or in the case of photons, be detected as gamma ray radiation [10]. However, for the parameter range considered here, these bounds are irrelevant because all modes have lifetimes under one year while the time scale of neutron star cooling is 10^5 years or more. While very young neutron stars may have a residual density of orbiting KK modes, these early environments are too noisy to allow detection of trace amounts of additional radiation.

4.2.2 Big Bang Nucleosynthesis

Another thermal source of light KK gravitons is the early universe. Gravitons can be produced in abundance at early times and then decay to all kinematically allowed Standard Model particles, affecting the delicate balance of Big Bang Nucleosynthesis (BBN). The standard model of nucleosynthesis matches measured relative abundances of the light elements very well and is sensitive to processes that take place in the early universe between $1-10^6$ s. KK gravitons which decay too slowly and are too abundant can upset this balance; we derive limits on the parameter space by requiring any decay product interactions to be subdominant to established rates at the time of decay.

The leading processes that affect BBN light element balance are proton and neutron interconversion and deuterium over- or under-production relative to He^4 . Electromagnetic (e, γ) as well as hadronic (π, K, p, n, \dots) decay products can contribute to these interconversions. These processes have been used to constrain other extra dimensional models as well as some supersymmetry models [23–28]. The bounds depend on the lifetime of the KK graviton, the type and total energy E_d of the decay products, and the abundance $Y_G = n_G/s$ of the gravitons.

For a given KK spectrum, the lifetime decreases rapidly with mode number n as $\tau \sim n^{-2}$ for low mass modes and $\tau \sim n^{-3}$ for higher modes, while the mass spacing is small, $\delta m \sim 0.1 m_1$, so the dominant bounds come from the first KK mode.

For $\alpha \lesssim 1$ GeV, the light modes are very weakly coupled and freeze-out while relativistic. Thus the abundance is not thermally suppressed [29],

$$Y_G = 0.278 \frac{g}{g_{*S}} \sim \mathcal{O}(1) \quad (40)$$

for each KK mode, where $g = 5$ is the number of internal degrees of freedom of the graviton and g_{*S} is the number of effectively massless degrees of freedom at freeze-out. Since the abundances are so high, there are significant limits even for short lifetimes.

There are bounds on electromagnetic decay products starting at $t \gtrsim 10^4$ s from the observed ratio of D to He⁴ and weaker bounds from the He⁴ to proton ratio Y_p as early as $t \gtrsim 10^2$ s [23, 24]. Since KK abundances are order 1, even these weak bounds can be used to constrain the parameter space. We use the bound $m_G Y_G e^{-t_{EM}/\tau} < 10^{-6}$ GeV at $t_{EM} \gtrsim 10^2$ s [24]. This limit is shown in orange in Fig. 3.

For heavier modes, hadronic decays are the limiting factor: for a particle of mass 100 GeV and dominant decays to hadrons, the bound on energy deposited is $m_G Y_G \lesssim 10^{-9}$ GeV at $t_H \gtrsim 0.1$ s [24]. For KK masses below 1 GeV, no nucleons are produced in decays. This weakens the bound, but not entirely: for mesons at temperatures above 1 MeV, the interaction length is comparable with the decay length, and a 1-10% of mesons induce charge exchange before decaying [25]. For decay times shorter than 1 s, mesons contribute to charge exchange, increasing He⁴ abundance, with an efficiency $\mathcal{E} \sim 10\%$ of baryons [30].

We impose $\mathcal{E} m_G Y_G e^{-t_H/\tau} \lesssim 10^{-9}$ GeV to satisfy the bounds above. Heavier modes, $m_n \gtrsim$ GeV, can decay to baryons which have stronger interactions with nuclei. However, the lifetimes of these modes are shorter and so the effects on BBN are smaller than from mesons at relevant times.

Additionally, very light modes with lifetimes longer than one second can change the number of relativistic degrees of freedom in the early universe which contribute to the entropy density. Massless particles have a significant effect on the rate of expansion of the universe during BBN, leading to different freeze-out times of nuclear reactions and different relative abundances of light species. Each KK graviton mode has 5 degrees of freedom and can have a large effect; thus we impose a hard limit of $\alpha \gtrsim 2$ MeV to exclude all masses below 1 MeV which would be effectively massless at the time of BBN.

For large extra dimensions, other cosmological bounds arise from overabundance of CMB photons or the over-closure of the universe [7]. These limits assume much longer lifetimes and are irrelevant here.

4.3 Fixed Target Experiments

Beyond astrophysical processes, we set direct limits on KK gravitons from ground-based laboratory experiments. In particular, fixed target beam dump experiments can be used to search for or rule out the presence of light gravitons. Two types of beam dump experiments—proton beam on target and electron beam on target—have been designed to search for axions as well as to measure neutrino oscillations [31–33]. More recently, interest in fixed target setups has been renewed by searches for dark gauge forces [34, 35]. KK gravitons can be produced in the beam collision with the target and travel through shielding; their decay products can then be measured in a detector downstream.

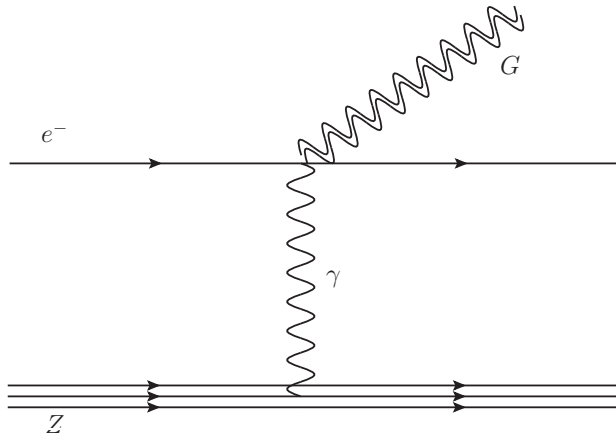


Figure 4: KK gravitron production off the electron beam in the field of target nuclei with atomic number Z .

Proton beams on target—used in many generations of neutrino oscillation experiments—create π s that decay to neutrinos. Gravitons can be produced in the collisions and have some probability to travel underground and decay inside the Cherenkov detector designed to detect neutrino interactions. The beam energy is high at tens to hundreds of GeV leading to higher production rates, but the probability for a graviton to decay in the volume of the detector is small.

Electron beam dump experiments on the other hand were designed specifically to search for decaying weakly coupled particles. The target is followed by shielding to stop other beam products, followed by a decay region. A detector measures decays of the weakly interacting particles into pairs of electrons, photons, and in some experiments muons.

To find current limits from beam dump experiments, there are two quantities to calculate: the number of gravitons produced over the duration of the experiment, and the probability that decay products of a single graviton will reach the detector and pass the experimental quality cuts.

The current leading limit comes from the E137 experiment at SLAC which dumped a 20 GeV electron beam onto a thin aluminum target followed by 200 m of shielding and a 200 m decay region. Limits from other electron beam dumps such as SLAC E141 and Fermilab E774 as well as proton beams MiniBoone, MINOS are weaker than the combined E137 bound and LHC bound discussed in Section 4.4.

New electron beam fixed target experiments have been proposed and some are in the process of being implemented. The heavy photon search, on schedule to begin data taking this year, may have a reach which extends beyond the current bounds.

Production The leading process for graviton production is gravitron production off the electron beam mediated by virtual photons in the field of target nuclei (Figure 4). The kinematics of the process at graviton energy small compared to beam energy $E_G \ll E$ are the same for any massive boson bremsstrahlung, and the model-dependent $2 \rightarrow 2$ process $e^- \gamma \rightarrow e^- G$ factors in the limit of low momentum transfer. We follow the calculation in [34] to compute the differential cross-section for graviton emission.

The production cross-section is given by the Weizsacker-Williams approximation [36], which relates the differential cross-section σ for the $2 \rightarrow 3$ process $e^- Z \rightarrow e^- Z G$ (Figure 4) to the $2 \rightarrow 2$ process $e\gamma \rightarrow eG$,

$$\frac{d\sigma}{dE_G d\cos\theta_G} = 2F_\gamma \frac{E x \beta_G}{1-x} \frac{d\sigma(e\gamma \rightarrow eG)}{dt} \Big|_{\min(-q^2)} \quad (41)$$

where $\beta_G = \sqrt{1 - \frac{m_G^2}{E^2}}$, $x = E_G/E$ is the fraction of the beam energy E carried by the graviton, and $F_\gamma = \frac{\alpha_{em}\chi}{\pi}$ is the effective photon flux sourced by the target atoms and is a function of atomic number characterized by $\chi \propto Z^2$. Here q is the momentum of the photon and the kinematics are evaluated at minimum momentum transfer in the $2 \rightarrow 3$ process.

The cross-section of the $2 \rightarrow 2$ process for producing KK mode n , $e^- \gamma \rightarrow e^- G$ is given by crossing symmetry from the graviton production process $e^+ e^- \rightarrow \gamma G$ [37],

$$\frac{d\sigma_{2 \rightarrow 2}}{dt} = \frac{\alpha_{em}}{16\Lambda_n^2} F_2 \left(\frac{t}{s}, \frac{m_G^2}{s} \right) \quad (42)$$

where

$$F_1(x, y) = \frac{-4x(x+1)(2x^2+2x+1) + (16x^3+18x^2+6x+1)y + (4x+1)y^3 - 6x(2x+1)y^2}{x(-x+y-1)}$$

$$F_2(x, y) = -(y-1-x) F_1\left(\frac{x}{y-1-x}, \frac{y}{y-1-x}\right) \quad (43)$$

At minimum momentum transfer we can express (51) with $2 \rightarrow 2$ cross-section (42) in terms of x , m_e/m_G , θ , beam energy E and graviton mass and coupling Λ_n^{-1} . To evaluate the expression we expand in two small parameters: the electron to graviton mass ratio m_e/m_G and the angle of graviton emission relative to the beam $\theta \lesssim (m_G/E)^{3/2}$. Integrating around $\theta = 0$ and keeping only the leading term in $\theta \rightarrow 0$ that gets regulated by either the finite mass of the electron or the finite mass of the graviton, $(m_G/E)^{3/2}$, we find the differential cross-section with respect to graviton energy,

$$\frac{d\sigma_n}{dx} = F_\gamma \beta_G \frac{\alpha_{em} (1-2x+2x^2) \log(1/\theta_{min})}{8\Lambda_n^2} \quad (44)$$

Then integrating with respect to x gives a total cross-section for producing mode n

$$\sigma_n = \frac{\alpha_{em}^2 \beta_G \chi}{12\pi \Lambda_n^2} \log(1/\theta_{min}) \quad (45)$$

For the E137 experiment with a thin aluminum target and beam energy of 20 GeV, $\log(1/\theta_{min}) \sim 3$ and $\chi \sim 5Z^2$, so

$$\sigma_1 = 2 \times 10^{-5} \text{ fb} \left(\frac{\alpha}{100 \text{ MeV}} \right) \left(\frac{M_5}{\text{TeV}} \right)^3 \quad (46)$$

$$\sigma_{10} = 10^{-3} \text{ fb} \left(\frac{\alpha}{100 \text{ MeV}} \right) \left(\frac{M_5}{\text{TeV}} \right)^3 \quad (47)$$

Decay and detection Knowing the production cross-section and kinematics of the system, we calculate the probability of decay products to enter the detector and take into account detector acceptances.

The detector acceptance depends on the angular size of the detector relative to the point z where the decay occurs as well as the energy fraction of the beam xE of the KK graviton. For a thin target like the one used in E137, the number of decays into with energy xE at a point z after the target is given by [34]

$$\frac{dN}{dxdz} = N_e n \frac{d\sigma_n}{dx} (e^{l_t/l_n} - 1) e^{-z/l_n} \epsilon_{vis} \quad (48)$$

where n is the number density of the target material, l_t is the target length, $l_n = \gamma v \tau_n$ is the decay length of the n^{th} KK mode in the lab frame, and ϵ_{vis} is the graviton branching fraction into modes visible in the detector (generally photons and electrons). For masses below $2m_\mu$, $\epsilon_{vis} = 2/3$ and for $m < 300 \text{ MeV}$, $\epsilon_{vis} = 6/11$ or $8/11$ depending on whether the detector is equipped with muon spectrometers.

The decay length depends strongly on the parameters and mode number:

$$l_1 = (4 \times 10^6 \text{ m}) \left(\frac{\alpha}{100 \text{ MeV}} \right)^{-5} \left(\frac{M_5}{\text{TeV}} \right)^3 \quad (49)$$

$$l_{n>10} = (4 \times 10^4 \text{ m}) \left(\frac{10}{n} \right)^4 \left(\frac{\alpha}{100 \text{ MeV}} \right)^{-5} \left(\frac{M_5}{\text{TeV}} \right)^3 \quad (50)$$

The optimal decay length is on the order of the baseline of the experiment; this allows for the largest production cross-section while maximizing the chance for the decay products to enter the detector.

We sum over all modes n to find the total number of expected events. The excluded yellow region in Figure 3 corresponds to 10 events in the E137 detector; integrating (48) against detector geometry and acceptances produces a 95% limit given that no events were observed over the course of the experiment.

4.4 Large Hadron Collider

4.4.1 Low Curvature Searches

Unlike systems sensitive to the low-mass and long-lived part of the KK graviton spectrum such as supernovae, BBN, and beam dumps, the LHC will be able to produce a multitude of states, possibly up to the heaviest mode at the cutoff Λ_{UV} . For spacing between states δm smaller than the resolution of the detector, the Linear Dilaton has many similarities at the LHC to one large flat extra dimension. However, while current bounds on ADD can provide approximate limits on the parameter space, they do not directly apply since the experimental analysis for 1 flat extra dimension has not been performed.

There are several important differences between one large, low curvature extra dimension and $\delta \geq 2$ large extra dimensions. First, the behavior of the cross-section as a function of energy

changes; the amplitude for $2 \rightarrow 2$ s -channel exchange processes with a KK intermediate state is

$$\mathcal{A} = \mathcal{S}(s) \left(T_{\mu\nu} T^{\mu\nu} - \frac{T_{\mu}^{\mu} T_{\nu}^{\nu}}{3} \right) \quad (51)$$

where

$$\mathcal{S}(s) = \frac{-i\pi}{M_5^3 \sqrt{s}} + \frac{2}{\Lambda_{UV}}, \quad (52)$$

while for $n = 2$ extra dimensions, $\mathcal{S}(s) \propto \ln(s/\Lambda_{UV}^2)$, and for $n > 2$, $\mathcal{S}(s) \propto \Lambda_{UV}^{n-2}$ and is independent of s [19]. Based on the fact that in $n \geq 2$ extra dimensions the signal cross-section does not fall with center of mass energy, the experimental signal regions have been selected to be at very high invariant masses [14–16,18]. For the linear dilaton geometry, the cross-section is inversely proportional to s and so the searches optimized for $\delta \geq 2$ are less effective. Furthermore, just for one extra dimension is the cross-section only weakly sensitive to the cutoff; in the remainder of the paper we take the cutoff to be $\Lambda_{UV} \simeq M_5$.

Second, in low curvature models gravitons have a short lifetime and can be produced on shell so the production cross-section is enhanced. In the narrow-width approximation, the enhancement is by a factor of $1/\epsilon$ where

$$\epsilon = \frac{\pi \Gamma_n}{2 \delta m_n} \Big|_{m_n=\sqrt{s}} = \frac{k}{2\pi} \left(\frac{\sqrt{s}}{M_5} \right)^3 \quad (53)$$

and k is an order one number that depends on the available decay modes of the graviton into Standard Model particles [19]. In fact, since the width is still much smaller than the mass splitting of states, on-shell production dominates over interference with SM processes. This increases the importance of processes with s -channel exchange, such as dilepton and diphoton final states.

Last, for the parameter range allowed by astrophysics and fixed target experiments, a vast majority of states decay immediately inside the detector, and at most a few tens of modes will have a displaced vertex decay. Thus the jet plus missing energy search which currently places the tightest bounds on one extra dimension, is no longer relevant. There is a small signal from the decay of gravitons to neutrinos, but the branching fraction is less than 4%. Since the cross-section scales as M_5^{-3} , this weakens the bound on M_5 from $j + \cancel{E}_T$ searches by a factor of 1/3.

A fraction of a percent of the modes for α on the order of several GeV will decay inside the detector with displaced vertices between 100 μm and several meters. While the displaced vertex signature is spectacular, it is a poor search channel: the total cross-section for displaced vertices are 1 fb or less while displaced vertex searches are currently sensitive to cross-sections of 1-100 pb and are tailored to supersymmetry signals, enforcing additional trigger requirements [38].

Without a missing energy or displaced vertex handle for searches, the experiments are limited to searches for an overall excess above Standard Model backgrounds in channels corresponding to graviton decay products: dijets, dileptons (muons and electrons), and diphotons. Current experimental searches focus on cut-and-count measurements in the invariant mass spectra: with the assumption that background falls more rapidly than signal with increasing center of mass energy, the signal region is simply defined with a lower bound on the dimuon (diphoton, dijet)

invariant mass. Then limits are set by comparing the observed and expected event counts in the signal region. Current searches have signal regions start at an invariant masses near 1 TeV, depending on the channel [14–16, 18].

Gravitons couple universally to the stress-energy tensor so branching fractions to SM particles only depend on the degrees of freedom of the decay products. Due to color factors, the leading decay is to jets; dijet final states are dominated by t -channel $uu \rightarrow uu$. However, even though the $pp \rightarrow G \rightarrow jj$ rate is higher than diphoton or dilepton, the sensitivity and reach to M_5 is worse because of large systematic uncertainties on the normalization and shape of jet distributions [5].

Potential reach in the dijet channel can be improved by considering observables with less systematic uncertainty, such as the angular distance between two final jets as proposed in [19]. However this analysis is least effective for one extra dimension, where the angular dependence is most similar to the Standard Model, resulting in a weak bound: $M_5 > 0.8$ TeV for the latest ATLAS results with 36 pb^{-1} [19, 39]. If the experimental collaborations release updated analyses, these limits may become competitive with current bounds from dileptons and diphotons and can provide another tool for characterizing the theory.

The cleaner dimuon and diphoton cut-and-count searches currently provide the most stringent bound on the low scale of gravity, M_5 . Gravitons have comparable decay rates to muons and photons, $\Gamma(G \rightarrow \gamma\gamma) = 2\Gamma(G \rightarrow \mu\mu)$, while Standard Model processes produce many more dimuons from Drell-Yan than diphotons. Thus, the bound to photons is stronger despite lower photon detection efficiencies and large uncertainties in the diphoton mass spectrum. Electron reconstruction has similar uncertainties to that of photons but electrons are produced in abundance through DY and so provide a weaker limit than either dimuons or diphotons.

To convert current experimental limits to bound on M_5 in the LD scenario, we model a generic small- $|\alpha|$ model at the LHC and derive a signal cross-section σ_s at invariant masses up to M_5 . For a high-energy collider, the 5-d curvature is irrelevant as long as $|\alpha| \ll M_5 \sim \text{TeV}$. This is due to the fact that high momentum is insensitive to curved space for $p^2 \gg \alpha^2$; thus high- n modes effectively see a flat extra dimension and have equal couplings. In the high-energy limit, both LD and low curvature RS KK spectra depend only on the 5-d Planck scale and the size of the “box” in which the gravitons propagate. The production cross-sections at high n are $\sigma_n \propto (r_c M_5^3)^{-1}$ and the models have identical phenomenology.

Using this intuition, we model a production scenario at the LHC with low curvature $|\alpha|$ as a sum over modes with $|\alpha| = 100 \text{ GeV}$ up to a cutoff at M_5 . The first mode, at 50 GeV, is below most detector energy cuts and the spacing between modes ranges from 0.1 to 5 GeV, well below the resolution of the detector. The events are generated in MadGraph 5.0 [17]. We verify that our results do not depend on the value of α at energies above $|\alpha|/2$. The decay width $\Gamma \ll \delta m$, and so there is no interference between the modes or with Standard Model particles in the s -channel. The dimuon invariant mass spectrum at the LHC for a background and signal example spectrum with $M_5 = 3 \text{ TeV}$, $|\alpha| = 100 \text{ GeV}$ after 30 fb^{-1} integrated luminosity at $\sqrt{s} = 7 \text{ TeV}$ is shown in Figure 1(b).

We consider the published bounds on signal cross-sections from experimental collaborations at 2.2 fb^{-1} integrated luminosity, $\sigma_s < 1.2 \text{ fb}$ for $m_{\mu\mu} > 1100 \text{ GeV}$ and $\sigma_s < 3.0 \text{ fb}$ for $m_{\gamma\gamma} > 900 \text{ GeV}$ [16, 18]. We take into account detector acceptances, cuts, and approximate NLO K-factor corrections, and find a bound from $pp \rightarrow \mu\mu$ to be $M_5 > 2.7 \text{ TeV}$ and a stronger bound

K factor	Diphotons		K factor	Dimuons	
	Signal Region			Signal Region	
	$M_{\gamma\gamma} > 900$	$M_{\gamma\gamma} > 500$		$M_{\mu\mu} > 1100$	$M_{\mu\mu} > 600$
1.6	3.1 TeV	4.8 TeV	1.3	2.7 TeV	3.5 TeV
1.0	2.5 TeV	4.1 TeV	1.0	2.5 TeV	3.2 TeV

Table 1: Current 95% CL limits on M_5 at 7 TeV after 2.2 fb^{-1} in diphoton and dimuon searches.

$pp \rightarrow \gamma\gamma$ to be $M_5 > 3.1 \text{ TeV}$ for $K = 1.6$ and $M_5 > 2.6 \text{ TeV}$ for $K = 1.0$. A summary of the limits is shown in Table 1.

However, we find that as the searches were optimized for $\delta \geq 2$ large extra dimensions, the tighter bounds would actually come by including some of the ‘control’ regions with lower invariant mass. From the published 7 TeV CMS studies [16, 18], we calculate an approximate exclusion from the 2.2 fb^{-1} diphoton spectrum of $M_5 \geq 4.1 \text{ TeV}$ for leading order production (K factor of 1.0) and 4.8 TeV for NLO production ($K = 1.6$) at 95% CL. We find a sub-leading bound of $M_5 \geq 3.2(3.5) \text{ TeV}$ for $K = 1.0(1.3)$ at 95% CL from the dimuon spectrum. The leading order graviton production bound of 4.1 TeV is shown in Figure 3. Without detailed knowledge of systematic uncertainties for these signal regions, our limits are an overestimate. Accurate limits can only be set by the experimental collaborations with a reconsideration of the signal and control regions and the systematic uncertainties at different energies.

4.4.2 Future Reach

The most promising avenue for exploring the low-curvature parameter space is the Large Hadron Collider. In this section we perform an analysis similar to that in Section 4.4.1 to find the ultimate reach in M_5 for low α with a center of mass energy $\sqrt{s} = 14 \text{ TeV}$ LHC. The best limits come from diphoton invariant mass measurements; dimuon searches are less effective but can provide an important confirmation in case of discovery.

We calculate signal and background spectra at $\sqrt{s} = 14 \text{ TeV}$ with MadGraph 5.0 [17]. For the diphoton channel, in addition to diphoton production $pp \rightarrow \gamma\gamma$, we approximate the contribution from jet conversion or misidentification in the $\gamma + \text{jet}$ and jet-jet channels as an up to 10% effect for $m_{\gamma\gamma} > 900 \text{ GeV}$. For concreteness we assume current experimental parameters: 22% background uncertainty, signal efficiency of $76.4 \pm 9.6\%$, a background K factor of 1.3, and the same isolation and η cuts as the current 7 TeV CMS studies [16]. Optimizing the reach for 10 fb^{-1} gives a signal region $m_{\gamma\gamma} > 1000 \text{ GeV}$, and for 100 fb^{-1} a signal region $m_{\gamma\gamma} > 1500 \text{ GeV}$.

For the dimuon channel we again assume current experimental parameters: 16% background uncertainty, signal efficiency of 90%, and the same isolation and η cuts as the current 7 TeV CMS studies [18]. In this case we find an optimal signal region $m_{\mu\mu} > 1100 \text{ GeV}$ at 10 fb^{-1} , and $m_{\mu\mu} > 1400 \text{ GeV}$ at 100 fb^{-1} .

For small curvature, although the jet plus missing energy channel would give the best reach for one extra dimension (up to 17 TeV for 100 fb^{-1}), without the missing energy signature the NLO reach is $M_5 \gtrsim 7.9 \text{ TeV}$ for 10 fb^{-1} and $M_5 \gtrsim 9.0 \text{ TeV}$ for 100 fb^{-1} . The detailed results for

K factor	Diphotons		K factor	Dimuons	
	Integrated Luminosity 10 fb ⁻¹	100 fb ⁻¹		Integrated Luminosity 10 fb ⁻¹	100 fb ⁻¹
1.6	7.9 TeV	9.0 TeV	1.3	6.6 TeV	7.8 TeV
1.0	6.7 TeV	7.7 TeV	1.0	6.1 TeV	7.1 TeV

Table 2: Future reach: 95% CL limits on M_5 for $|\alpha| \ll M_5$ at the $\sqrt{s} = 14$ TeV LHC.

$\sqrt{s} = 14$ TeV are listed in Table 2.

Without detailed experimental background studies at $\sqrt{s} = 14$ TeV the limits are only approximate. Nevertheless, the total signal cross-section σ_s scales as M_5^{-3} so our limits are only weakly sensitive to errors in background modeling or systematics: a change in the background cross-section in the signal region by 50% results in a 10% change in M_5 reach.

5 Low Curvature Randall-Sundrum

For low curvature Randall-Sundrum models, the same sets of limits apply as in the low curvature linear dilaton model. We apply our analysis of Sections 4.2–4.4 to the scenario presented in [5] and consider the two-parameter space of the 5-d Planck scale M_5 and first KK mass m_1 (Figure 5). In this case, the coupling is independent of mode number and is given by

$$\Lambda = (2.8 \times 10^5 \text{ GeV}) \left(\frac{m_1}{50 \text{ MeV}} \right)^{1/2} \left(\frac{M_5}{\text{TeV}} \right)^{-3/2} \quad (54)$$

and the KK mass spectrum is $m_n = \frac{x_n}{x_1} m_1$, where

$$x_n = \beta_n - \frac{3}{8\beta_n} + \frac{3}{128\beta_n^3} - \frac{1179}{5120\beta_n^5} + \dots, \quad \beta_n = \left(n + \frac{1}{4} \right) \pi \quad (55)$$

Unlike the linear dilaton geometry, in low curvature RS the spacing between KK modes is parametrically the same as the mass gap m_1 ; for a fixed m_1 there are fewer modes up to the cutoff than in LD and each mode is more strongly coupled than in LD. In the case of BBN for example, the contributions of the first several modes to the hadronic limit are visible individually (Fig. 5).

Since each KK mode in low curvature RS is more strongly coupled than the corresponding mode in LD, the reach with beam dump experiments extends to higher curvature. In contrast, the shorter decay lengths and stronger couplings significantly weaken bounds from supernovae and BBN: there are no constraints from astrophysics at TeV-scale M_5 down to a mass gap of 1 MeV. The LHC on the other hand is insensitive to the details of the spectrum, so the collider bounds and future reach (Table 2) on M_5 are identical in low curvature RS and LD models.

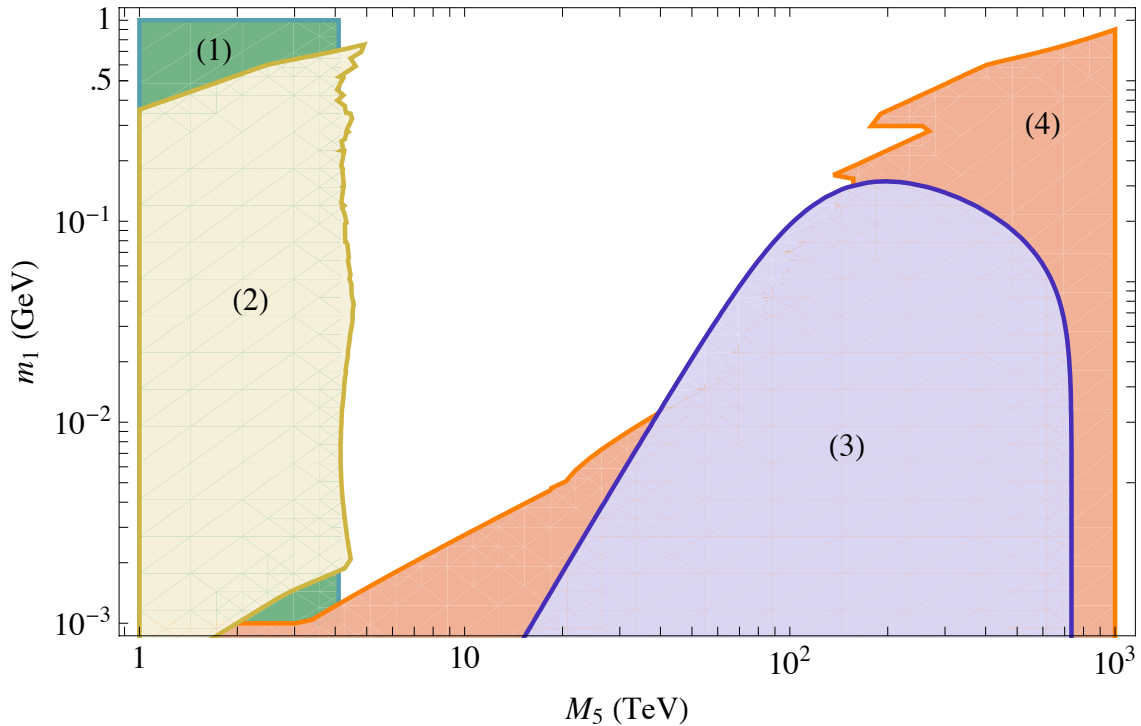


Figure 5: Current Bounds on Low Curvature RS. (1) Green: LHC limits at $\sqrt{s} = 7 \text{ TeV}$ after 2 fb^{-1} integrated luminosity, (2) yellow: 10 events in the E137 electron beam dump experiment (zero events were observed over the course of the experiment), (3) purple: energy flux from Supernova 1987A, (4) orange: BBN electromagnetic, hadronic, and entropy bounds.

6 Discussion and Conclusions

We have studied the phenomenology of an extra dimension with a linear dilaton background, inspired by possibilities of Little String Theory at a TeV. The linear dilaton background gives rise to a unique gapped mass spectrum, where the curvature $|\alpha|$ in the extra dimension lifts the graviton KK spectrum. The corresponding radion phenomenology is studied in a complementary paper [40]. Other states may also result from LST at a TeV; these depend on the compactification details and can be strongly coupled, so we do not consider them here [4].

For large curvatures $|\alpha|$ close to the five dimensional Planck scale M_5 , the LHC can provide a wealth of information. KK modes are separated by more than the resolution of the LHC, and if one resonance is detected it will be possible to study a tower of light resonances by the end of the LHC run. The mass gap of size $|\alpha|/2$ and mode-number-dependent coupling Λ_n can identify an excess at the LHC as resulting from the linear dilaton scenario. The resonances can be clearly identified as gravitons by studying branching fractions to muons, photons, electrons, and jets, which are set by the universal coupling of the KK modes to the stress-energy tensor. In addition the spin of the resonances can be established with sufficient statistics by measuring angular correlations of decay

products [41].

Another possibility is one large extra dimension at the LHC: for low curvatures $|\alpha| \ll M_5$, the LHC is insensitive to details of the graviton spectrum. In this region of parameter space the contribution of KK modes will appear as a continuous excess with the same dependence on center of mass energy as a large flat extra dimension. As we demonstrate in Section 4, the small mass gap avoids exclusions from supernovae and BBN, and as each KK mode is much more strongly coupled than M_{Pl}^{-1} , the gravitons decay in the detector and do not carry away missing energy. This possibility has not been included in experimental analyses; we calculate the current limit based on published data and demonstrate that as the searches have not been optimized with one large extra dimension in mind, the reach of the searches could be improved by relaxing the invariant mass cut of the signal region.

The phenomenology of low curvature RS models is similar to that of the low curvature linear dilaton, and we apply our analysis to this case as well. We find that the first mode of the theory can be as light at 1 MeV and avoid astrophysical limits. The best avenues for discovery are new beam dump experiments and the LHC at increased center-of-mass energy.

The most promising discovery channel at the LHC is the diphoton invariant mass spectrum due to low Standard Model backgrounds at high energies, followed by dimuons. For large curvatures, a 14 TeV LHC can reach $M_5 \sim 5$ TeV depending on the strength of the coupling set by $|\alpha|$. For small curvature, the reach goes up to 7.9 TeV for 10 fb^{-1} and 9.0 TeV for 100 fb^{-1} .

If a signal corresponding to one large extra dimension is observed at the LHC, one exactly flat extra dimension can clearly be excluded by lack of missing energy signatures. Further information about the detailed geometry will require low-energy experiments, since without sensitivity to individual resonances it is impossible to distinguish low curvature theories. For a sufficiently low 5-d gravity scale, fixed target experiments could detect individual, longer lifetime states; for example, the currently commissioned Heavy Photon Search proposed to search for light dark matter [34, 42] can study coupling strengths and lifetimes of KK gravitons with masses of up to several GeV.

7 Acknowledgements

We thank Ignatios Antoniadis, Savas Dimopoulos, Amit Giveon, Natalia Toro, and especially Asimina Arvanitaki for useful discussions. MB is supported in part by the NSF Graduate Research Fellowship under Grant No. DGE-1147470. This work was supported in part by ERC grant BSMOXFORD no. 228169.

References

- [1] N. Arkani-Hamed, S. Dimopoulos, and G. Dvali, *Physics Letters B* **429**, 263 (1998), hep-ph/9803315.
- [2] L. Randall and R. Sundrum, *Physical Review Letters* **83**, 3370 (1999), hep-ph/9905221.

- [3] I. Antoniadis, S. Dimopoulos, and A. Givon, *Journal of High Energy Physics* **2001**, 055 (2001), hep-th/0103033.
- [4] I. Antoniadis, A. Arvanitaki, S. Dimopoulos, and A. Givon, *Phys. Rev. Lett.* **108**, 081602 (2012), 1102.4043.
- [5] G. F. Giudice, T. Plehn, and A. Strumia, *Nuclear Physics B* **706**, 455 (2005), hep-ph/0408320.
- [6] N. Arkani-Hamed, M. Porrati, and L. Randall, *Journal of High Energy Physics* **2001**, 017 (2001), hep-th/0012148.
- [7] L. Hall and D. Smith, *Physical Review D* **60**, 10 (1999), hep-ph/9904267.
- [8] S. Cullen and M. Perelstein, *Physical Review Letters* **83**, 268 (1999), hep-ph/9903422.
- [9] C. Hanhart, D. R. Phillips, S. Reddy, and M. J. Savage, *Nucl. Phys.* **B595**, 335 (2001), 0007016.
- [10] S. Hannestad and G. Raffelt, *Physical Review D* **67** (2003), hep-ph/0304029.
- [11] E. Adelberger *et al.*, *Physical Review Letters* **98**, 13 (2007).
- [12] CMS Collaboration, A. Everett, *AIP Conf.Proc.* **1200**, 701 (2010).
- [13] ATLAS Collaboration, G. Aad *et al.*, (2009), 0901.0512.
- [14] ATLAS Collaboration, G. Aad *et al.*, (2011), 1112.2194.
- [15] ATLAS Collaboration, G. Aad *et al.*, *Phys.Rev.Lett.* **107**, 272002 (2011), 1108.1582.
- [16] CMS Collaboration, S. Chatrchyan *et al.*, (2011), 1112.0688.
- [17] J. Alwall, M. Herquet, F. Maltoni, O. Mattelaer, and T. Stelzer, *JHEP* **1106**, 128 (2011), 1106.0522.
- [18] CMS Collaboration, S. Chatrchyan *et al.*, (2012), 1202.3827.
- [19] R. Franceschini, P. Paolo Giardino, G. F. Giudice, P. Lodone, and A. Strumia, *Journal of High Energy Physics* **2011**, 16 (2011), 1101.4919.
- [20] T. Han, J. Lykken, and R.-J. Zhang, *Physical Review D* **59**, 1 (1999).
- [21] J. Bijnens and M. Maul, *JHEP* **0010**, 003 (2000), hep-ph/0006042.
- [22] G. G. Raffelt, *Ann.Rev.Nucl.Part.Sci.* **49**, 163 (1999), hep-ph/9903472.
- [23] R. Cyburt, J. Ellis, B. Fields, and K. Olive, *Physical Review D* **67**, 40 (2003), astro-ph/0211258.
- [24] M. Kawasaki, K. Kohri, and T. Moroi, *Physical Review D* **71**, 94 (2005), astro-ph/0408426.

- [25] K. Jedamzik, *Physical Review D* **74**, 24 (2006), hep-ph/0604251.
- [26] M. Kawasaki, K. Kohri, T. Moroi, and A. Yotsuyanagi, *Physical Review D* **78**, 27 (2008), 0804.3745.
- [27] S. Bailly, K. Jedamzik, and G. Moulhaka, *Physical Review D* **80**, 13 (2009), 0812.0788.
- [28] A. Arvanitaki, C. Davis, P. Graham, A. Pierce, and J. Wacker, *Physical Review D* **72**, 10 (2005), hep-ph/0504210.
- [29] E. W. Kolb and M. S. Turner, *The Early Universe* (Addison-Wesley Publishing Company, 1988).
- [30] M. Reno and D. Seckel, *Phys.Rev.* **D37**, 3441 (1988).
- [31] MINOS Collaboration, P. Adamson *et al.*, *Phys.Rev.* **D84**, 071103 (2011), 1108.1509.
- [32] Kamiokande Collaboration, K. Bays *et al.*, (2011), 1111.5031.
- [33] J. Bjorken *et al.*, *Physical Review D* **38**, 3375 (1988).
- [34] J. Bjorken, R. Essig, P. Schuster, and N. Toro, *Physical Review D* **80**, 14 (2009), 0906.0580.
- [35] B. Batell, M. Pospelov, and A. Ritz, *Phys.Rev.* **D80**, 095024 (2009), 0906.5614.
- [36] Y.-S. Tsai, *Phys.Rev.* **D34**, 1326 (1986).
- [37] G. F. Giudice, R. Rattazzi, and J. D. Wells, *Nuclear Physics* **B544**, 3 (1999), hep-ph/9811291.
- [38] ATLAS Collaboration, P. Jackson, (2011), 1112.0369.
- [39] ATLAS Collaboration, G. Aad *et al.*, *New J.Phys.* **13**, 053044 (2011), 1103.3864.
- [40] P. Cox and T. Gherghetta, *Radion Dynamics and Phenomenology in the Linear Dilaton Model*, To appear.
- [41] J. Hewett and M. Spiropulu, *Annual Review of Nuclear and Particle Science* **52**, 397 (2002).
- [42] A. Grillo *et al.*, *HPS Heavy Photon Search: A Proposal to Search for Massive Photons at Jefferson Laboratory*, 2010.